revista principia

ISSN 2447-9187

https://doi.org/10.18265/2447-9187a2025id8878

ORIGINAL ARTICLE

SUBMITTED February 7, 2025

APPROVED May 19, 2025

PUBLISHED ONLINE June 16, 2025

FINAL FORMATTED VERSION March 11, 2025

ASSOCIATE EDITOR
Dr. Koje Daniel Vasconcelos Mishina

Influence of Friction Stir Welding (FSW) parameters on the thermal cycles and mechanical properties of AA7075-T651 joints

Oclávio Coutinho dos Santos [1] *

José Wallisson de Abreu Souza [2]

Theophilo Moura Maciel [3]

Marco Antonio dos Santos [4]

João Baptista da Costa Agra de Melo [5]

Raphael Henrique Falcão de Melo [6]

[1] oclaviosantos@hotmail.com
[2] wallisson1215@hotmail.com
[3] theophilo.maciel@ufcg.edu.br
[4] marco.antonio@professor.ufcg.edu.br
[5] baptista.agra@hotmail.com
Federal University of Campina Grande (UFCG), Campina Grande, Paraíba, Brazil

[6] raphael.melo@ifpb.edu.br
Federal Institute of Paraíba (IFPB), Itabaiana, Paraíba, Brazil

* *Corresponding author.*

ABSTRACT: Aluminum alloys are widely used in the transportation sector due to their favorable characteristics and mechanical properties, which meet the growing demand for high-performance vehicles with enhanced autonomy. The 7XXX series is particularly notable among these alloys, especially in the aeronautical industry. The AA7075-T651 alloy was chosen for this study because of its high mechanical strength, low density, and superior corrosion resistance in comparison to other aluminum alloys, typically recommended for aeronautical and aerospace applications. However, its use is constrained when employing conventional welding techniques, mainly due to weldability challenges. To broaden the applicability of this alloy to other structural components, the development of solid-state joining methods is essential. The low weldability of these alloys under fusion-based techniques is linked to the rapid vaporization of zinc and magnesium, primary alloying elements, that results in pore formation in the weld metal, thereby compromising joint integrity. Friction Stir Welding (FSW), a solid-state joining process, offers a promising alternative, effectively addressing these limitations. Since the mechanical properties of welded joints in heat-treatable aluminum alloys are significantly influenced by thermal exposure during welding, it is crucial to assess the temperature distribution throughout the FSW process and establish correlations with the thermal cycles experienced by the joints. In this study, AA7075-T651 alloy plates were welded under various process parameters: welding speeds of 117 mm/min and 47 mm/min, along with tool rotation speeds of 1,585 rpm and 470 rpm, using a threaded cylindrical tool made of H13 steel. Uniaxial tensile testing, macro- and microstructural characterization, Vickers hardness measurements, and thermal cycle monitoring using K-type thermocouples were performed. The highest peak temperatures, nearing 375 °C, were recorded under elevated welding and tool rotation speeds (117 mm/min and 1,585 rpm, respectively). In contrast, joints produced at lower welding (47 mm/min) and tool rotation speeds (470 rpm) displayed lower peak temperatures (~324 °C), reduced cooling rates (~3 °C/s), and enhanced mechanical performance, with ultimate tensile strength (UTS) reaching 353 MPa. Conversely, joints manufactured under higher energy input conditions exhibited brittle behavior and significantly lower UTS values (~176 MPa), attributed to excessive heat input and the accelerated thermal cycles involved.

Keywords: AA7075-T651 aluminum alloys; friction stir welding; mechanical properties; thermal cycles.

ISSN 2447-9187

Influência dos parâmetros da soldagem por fricção e agitação nos ciclos térmicos e propriedades mecânicas das juntas AA7075-T651

RESUMO: *As ligas de alumínio são amplamente utilizadas no setor de transportes devido às suas características e propriedades mecânicas favoráveis, que atendem à crescente demanda por veículos de alto desempenho com maior autonomia. A série 7XXX se destaca particularmente entre essas ligas, especialmente na indústria aeronáutica. A liga AA7075-T651 foi escolhida para este estudo devido à sua alta resistência mecânica, baixa densidade e resistência à corrosão superior em comparação com outras ligas de alumínio tipicamente recomendadas para aplicações aeronáuticas e aeroespaciais. No entanto, seu uso é limitado quando se empregam técnicas de soldagem convencionais, principalmente devido a desafios de soldabilidade. Para ampliar a aplicabilidade dessa liga a outros componentes estruturais, o desenvolvimento de métodos de união em estado sólido é essencial. A baixa soldabilidade dessas ligas sob técnicas baseadas em fusão deve-se à rápida vaporização de zinco e magnésio, elementos-chave da liga, que resulta na formação de poros no metal de solda, comprometendo a integridade da junta. A Soldagem por Fricção e Mistura (SFM), um processo de soldagem no estado sólido, oferece uma alternativa promissora, abordando efetivamente essas limitações. Como as propriedades mecânicas das juntas soldadas em ligas de alumínio tratáveis termicamente são significativamente influenciadas pela exposição térmica durante a soldagem, é crucial avaliar a distribuição de temperatura ao longo do processo SFM e estabelecer correlações com os ciclos térmicos experimentados pelas juntas. Neste estudo, chapas de liga AA7075-T651 foram soldadas sob vários parâmetros de processo: velocidades de soldagem de 117 mm/min e 47 mm/min, juntamente com velocidades de rotação da ferramenta de 1.585 rpm e 470 rpm, usando uma ferramenta cilíndrica com rosca feita de aço H13. Ensaios de tração uniaxial, caracterização macro e microestrutural, medições de dureza Vickers e monitoramento do ciclo térmico usando termopares do tipo K foram realizados. As temperaturas de pico mais altas, próximas a 375 °C, foram registradas sob velocidades elevadas de soldagem e rotação da ferramenta (117 mm/min e 1.585 rpm, respectivamente). Em contraste, juntas produzidas com velocidades de soldagem (47 mm/min) e rotação da ferramenta (470 rpm) mais baixas apresentaram temperaturas de pico mais baixas (~324 °C), taxas de resfriamento reduzidas (~3 °C/s) e melhor desempenho mecânico, com resistência à tração final (RTF) atingindo 353 MPa. Por outro lado, juntas fabricadas sob condições de maior aporte energético apresentaram comportamento frágil e valores de RTF significativamente menores (~176 MPa), atribuídos ao aporte térmico excessivo e aos ciclos térmicos acelerados envolvidos.*

Palavras-chave: *ciclos térmicos; ligas de alumínio AA7057-T651; propriedades mecânicas; soldagem por fricção e mistura.*

1 Introduction

Friction Stir Welding (FSW), developed in 1991 by The Welding Institute (TWI) in the United Kingdom, is a solid-state welding technique that joins materials through the combined effects of frictional heat and mechanical plastic deformation. The process uses a rotating cylindrical tool with a protruding pin, which traverses the joint line between two clamped base materials. Friction between the tool and the material generates heat, softening the material near the joint. The plasticized material is then stirred by the rotating tool, inducing intense plastic flow and mechanical mixing across the interface, thereby producing a solid-state bond between the components (Kim *et al*., 2020).

FSW has emerged as a solution to several limitations associated with conventional fusion welding techniques, particularly in materials with low weldability (Cintra Filho *et al*., 2018). In welding processes, it is generally assumed that materials with similar physical and chemical properties are joined, as the process itself can lead to strength reduction. Similar welding refers to the joining of materials with nearly identical compositions and mechanical behavior, resulting in more predictable metallurgical transformations and performance under thermal cycling, reducing the risk of forming detrimental intermetallic phases.

In contrast, dissimilar welding involves the joining of materials with significant differences in chemical composition, physical properties, or microstructure. This type of welding presents additional challenges, such as mismatched melting points, differences in thermal expansion coefficients, and the formation of brittle intermetallic compounds, all of which may compromise joint quality and mechanical integrity.

Heat-treatable aluminum alloys from the 2XXX, 6XXX, and 7XXX series are particularly sensitive to thermal cycling. Fusion welding of these alloys often results in a significant reduction in mechanical strength due to the formation of brittle interdendritic and eutectic phases, oxide inclusions, pore generation, and microstructural changes caused by the diffusion and redistribution of alloying elements during solidification (Colaço *et al*., 2020; Yang *et al*., 2018).

The AA7075-T651 alloy was chosen for this study given its high strength-to-weight ratio and superior corrosion resistance compared to other aluminum alloys commonly used in aerospace applications, such as AA2024. This alloy is extensively used in manufacturing critical components in the aerospace industry, including fuselage structures, stringers, and pressure-resistant assemblies in aircraft like the Airbus A380. According to Gao *et al*. (2020), the lightweight and cost-effective nature of AA7075 has also led to its increasing adoption in the automotive and civil infrastructure sectors.

However, due to the alloy's low weldability when fusion-based welding is employed, which is attributed to the rapid vaporization of zinc and magnesium during processing, there is a strong tendency for pore formation in the weld zone, Ardika *et al*. (2021) states that defects such as porosity are a factor in the reduction of some mechanical properties such as toughness, fatigue resistance and ductility of welded joints. These defects can considerably diminish the structural performance of the joint. Therefore, developing efficient solid-state joining techniques, such as FSW, is crucial to broaden the use of AA7075 in structural applications. As a solid-state process, FSW decreases the occurrence of metallurgical defects typically associated with fusion welding, making it a promising alternative for this class of alloys. This process uses a tool consisting of a pin and a shoulder. This tool is gradually inserted with a determined rotation between two firmly fixed plates. During the welding process, the shoulder of the tool makes strong contact with the surface of the plates, while the axial force is applied. Meanwhile, the tool moves

between the plates, producing heat from friction and thus joining them (Akbari; Asadi; Sadowski, 2023).

Several parameters influence the quality of FSW joints, including tool rotation speed, welding speed, and axial force. These variables directly affect the thermal profile and, consequently, the resulting mechanical properties. Wu *et al*. (2019) states that if the welding parameters are not chosen appropriately, it can generate excess heat, leading to welding defects. Furthermore, Silvestri *et al*. (2024) states that monitoring the temperature during the process is essential to obtain efficient welding, being a fundamental element for preliminary detection of welding defects and tool wear. Thus, monitoring and analyzing thermal cycles during the welding process are essential for understanding mass transport mechanisms, phase transformations, and their effects on joint integrity.

Previous research has highlighted the importance of thermal cycle investigation in FSW, given its impact on plastic flow behavior, microstructural evolution, and residual stress development. Wu *et al*. (2019) reinforces the importance of monitoring the temperature close to the tool during the process, as the rotation speed has significant influences during the welding process. Understanding the phenomena associated with heat generation and dissipation is fundamental for process optimization and the production of high-performance joints. Furthermore, the transportation industry increasingly demands higher welding speeds to enhance productivity and maintain competitiveness (Buglioni; Tufaro; Svoboda, 2015).

The present study investigates the influence of thermal cycles on the mechanical performance of similar AA7075-T651 aluminum alloy joints produced by FSW. Peak temperatures and cooling rates were measured during the welding process and correlated with the mechanical behavior of the joints. Additionally, the study examines how thermal cycles affect the formation of macro-defects such as wormholes and kissing bonds, and how these discontinuities impact the structural integrity of the welds. Special emphasis is placed on the influence of key process parameters, namely, tool rotation speed and welding speed, as they directly determine the heat input during the FSW process.

The remainder of this article is organized as follows: Section 2 details the materials and experimental procedures. Section 3 presents the results of the visual inspection, thermal cycle analysis, macro- and microstructural characterization, Vickers hardness testing, uniaxial tensile testing, and fractographic analysis. Finally, Section 4 summarizes the main findings of the study.

2 Materials and methods

This study employed 7075-T651 aluminum alloy sheets with dimensions of 60 mm × 120 mm × 6 mm to produce eight test specimens. The chemical composition of the plates, as provided by the manufacturer, is presented in Table 1.

Table 1 ▼
Chemical composition of AA7075-T651 (% by weight).
Source: Guler et al. (2019)

Cr	Cu	Fe	Mg	Mn	Si	Ti	Zn	Zr+Ti	Others	Al
0.18	1.5	0.19	2.5	0.1	0.1	0.1	5.8	0.25	0.05	Balance

The welding operations were carried out using a PROMILL FU-300-E milling machine. The initial welding parameters were based on the study by Lima *et al*. (2022). From that reference, parameters known to produce both sound and defective joints were

selected to evaluate the influence of the thermal cycle on defect formation, potentially due to alterations in the material's plastic flow during the welding process.

The impact of tool rotation speed, welding speed, and tool tilt angle was examined, as summarized in Table 2. These parameters were chosen because, according to Lima *et al*. (2022), they significantly influenced mechanical performance, particularly due to the occurrence of macro-defects typical in friction welding, such as wormholes and kissing bonds.

Table 2 ▶
Welding parameters.
Source: research data

Joint	υ =Welding speed (mm/min)	Ω =Tool rotation speed (RPM)	Θ = Tool tilt (°)
1	47	470	1
2	117	1,585	1
3	47	470	3
4	117	1,585	3

Figure 1 ▼
Welding tool (dimensions in mm).
Source: authors' archive

The welding tool used in the FSW process was machined from H13 tool steel. It featured a threaded cylindrical pin with a rounded tip, measuring 5.5 mm in length and 6 mm in diameter, and a shoulder with a diameter of 16 mm, as illustrated in Figure 1.

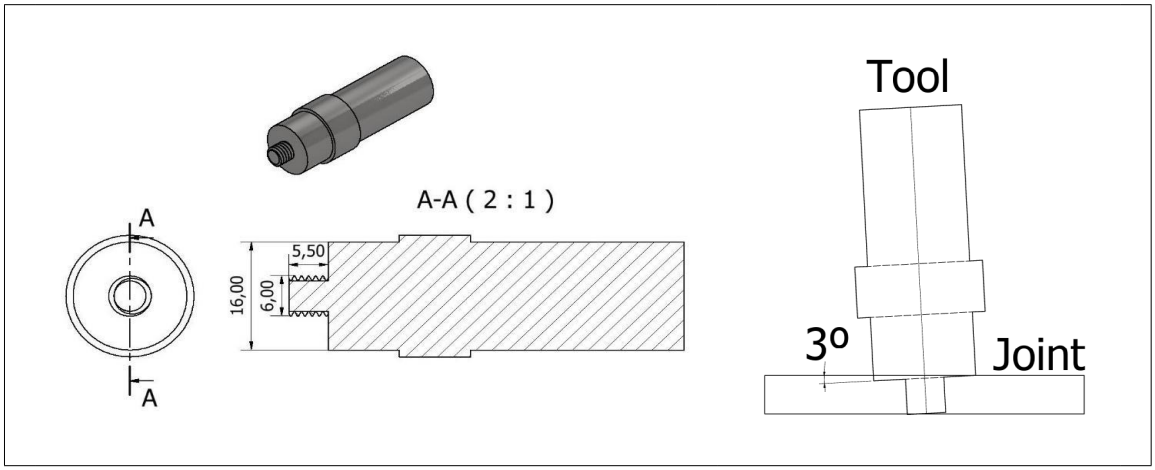

The thermal cycles were monitored using an Agilent data acquisition system, model 34970A. Type K thermocouples were employed and installed within the plates as shown in Figure 2. The thermocouples were inserted into holes at half the plate thickness (3 mm), positioned 10 mm and 12 mm from the weld interface and centerline, respectively, following the methodology described by Li *et al*. (2023). To avoid damage, the thermocouples were placed at positions slightly offset from the tool path, thus avoiding areas of intense agitation caused by the pin and shoulder. They were positioned on both the advancing and retreating sides of the joint. According to Bhukya *et al*. (2023), this arrangement provides a better understanding of the thermal cycles. The thermocouples were secured within the holes using high-temperature thermal adhesive tape (rated to 500 °C) and reinforced with electrical tape. The hole diameter was made as close to the thermocouple diameter (1 mm) to ensure a tight fit without gaps.

Figure 2 ▶
Thermocouples positions in the welded joint.
Source: authors' archive

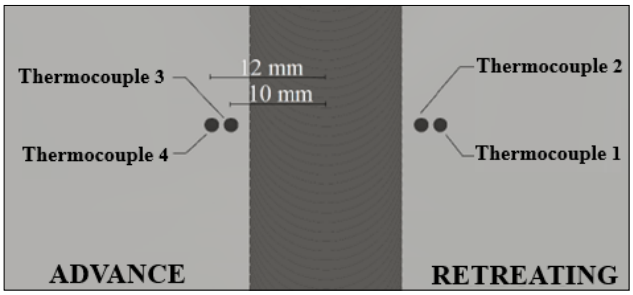

Figure 3 ▼
(a) Tensile test specimen by ASTM E8/E8M-16, (b) microhardness test specimen, and (c) extraction of samples for microhardness testing (dimensions in mm).
Source: authors' archive

Uniaxial tensile tests were performed on all welded joints, with three specimens tested per condition, enabling the calculation of the mean value and standard deviation. The tests were carried out using an MTS-810 universal testing machine at a crosshead speed of 1 mm/min until specimen failure. Figure 3a illustrates the geometry of the tensile test specimen.

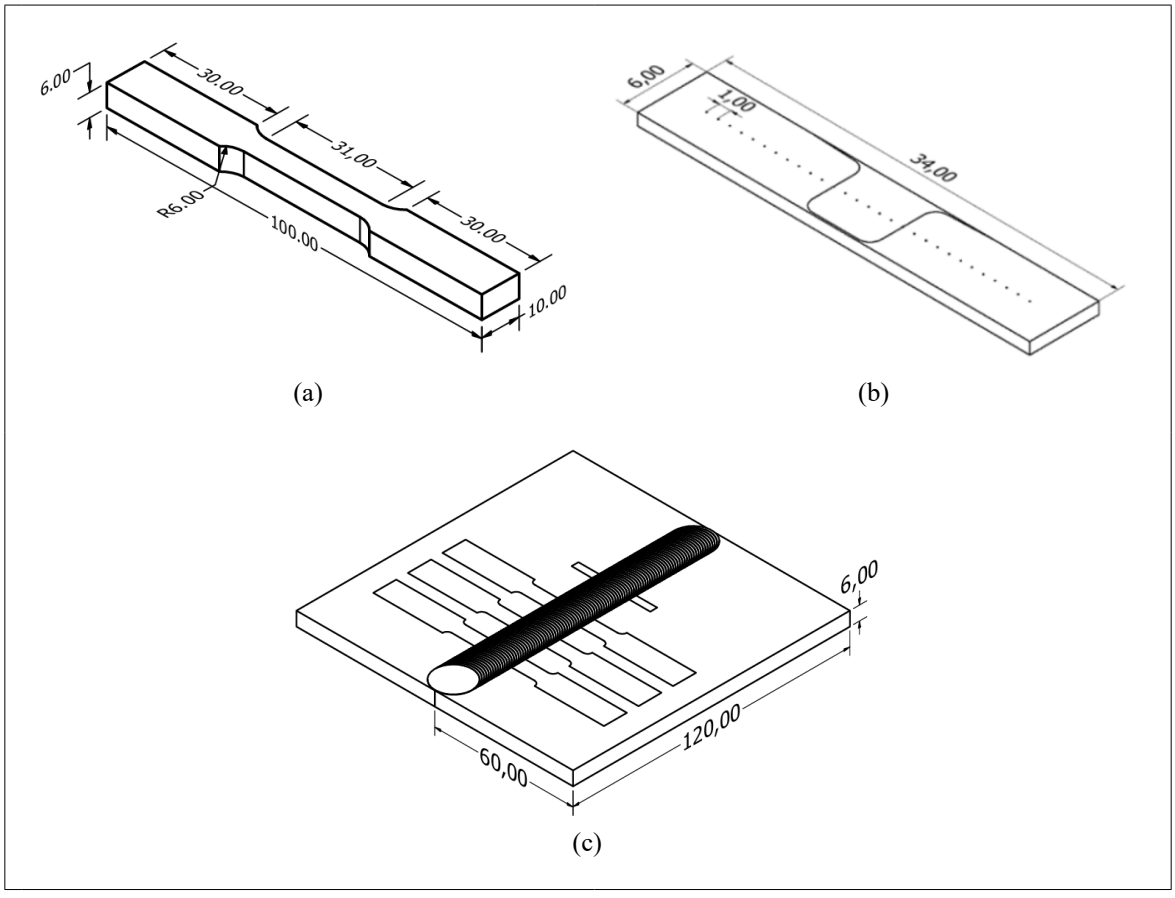

For microstructural analysis, specimens with the dimensions shown in Figure 3b were prepared and embedded in cold-cured acrylic resin. The samples were sequentially ground with silicon carbide abrasive papers of 220, 400, 600, 800, 1,200, and 2,200 grit, followed by polishing with 1 µm diamond paste. Surface conditions were inspected under an optical microscope after each preparation step.

Final polishing was carried out using 0.4 µm colloidal silica, and the specimens were etched with Keller's reagent for 60 seconds. The cross-sections of the welded joints were examined across the stir zone, Thermomechanically Affected Zone (TMAZ), and Heat-Affected Zone (HAZ).

The objective was to evaluate the microhardness profile extending from the stir zone to the base metal (BM) on both the advancing and retreating sides of the joints.

Microhardness measurements were conducted using a FutureTech FM-700 digital Vickers microhardness tester, applying a 200 gf load for 15 seconds. Indentations were spaced 1 mm apart. The indentation pattern is illustrated in Figure 3b, and specimens were extracted from the welded region as shown in Figure 3c.

Fractographic analysis was performed on the fractured surfaces after the tensile tests, using a VEGA3 SBH scanning electron microscope (SEM) at magnifications ranging from 100× to 1000×, to identify fracture features and defects that could contribute to premature failure.

3 Results and discussions

The results and discussion analyzed the results of the joints welded by the FSW process, together with the results of the mechanical tests to ascertain their effects and impacts on the results of the welded joints.

3.1 Visual analysis

A visual examination of all four welded joints, produced using different welding parameters as detailed in Table 3, was carried out to identify possible surface defects such as lack of penetration, surface irregularities, voids or tunnels, and excess burr formation.

Table 3 ▶
Joints welded using the FSW process.
Source: authors' archive

Joint	Top view of weld	Parameters
1		ω: 470 rpm υ: 47 mm/min θ: 1°
2		ω: 1,585 rpm υ: 117 mm/min θ: 1°
3		ω: 470 rpm υ: 47 mm/min θ: 3°
4		ω: 1,585 rpm υ: 117 mm/min θ: 3°

It was observed that joints 1 and 2 exhibited a greater amount of burr compared to the joints welded under similar parameters but with a higher tilt angle. This suggests that a lower tilt angle may promote increased burr formation in welded joints, likely due

to a higher normal force being applied in the stir zone (SZ), which facilitates greater material displacement from the center of the SZ. According to Colaço *et al*. (2020), burr formation at the sides of the weld is possibly caused by the high magnitude of axial force (Z-direction) applied during welding, leading to material loss that is later pushed to the sides as the tool advances. Additionally, tool rotation speed may influence burr generation: at high speeds, centrifugal forces acting on the material in the stir zone may disperse material outward. High welding speeds and inadequate tool geometries may further exacerbate this defect (Threadgill *et al*., 2009).

3.2 Welding thermal cycle

Figures 4 and 5 illustrate the thermal cycles of joints 1 and 3, and joints 2 and 4, respectively. Higher temperatures were recorded by thermocouple 3 in all joints, as it was positioned closer to the stir zone.

Figure 4 ▶
Thermal cycles of joints 1 (a) and 3 (b).
Source: research data

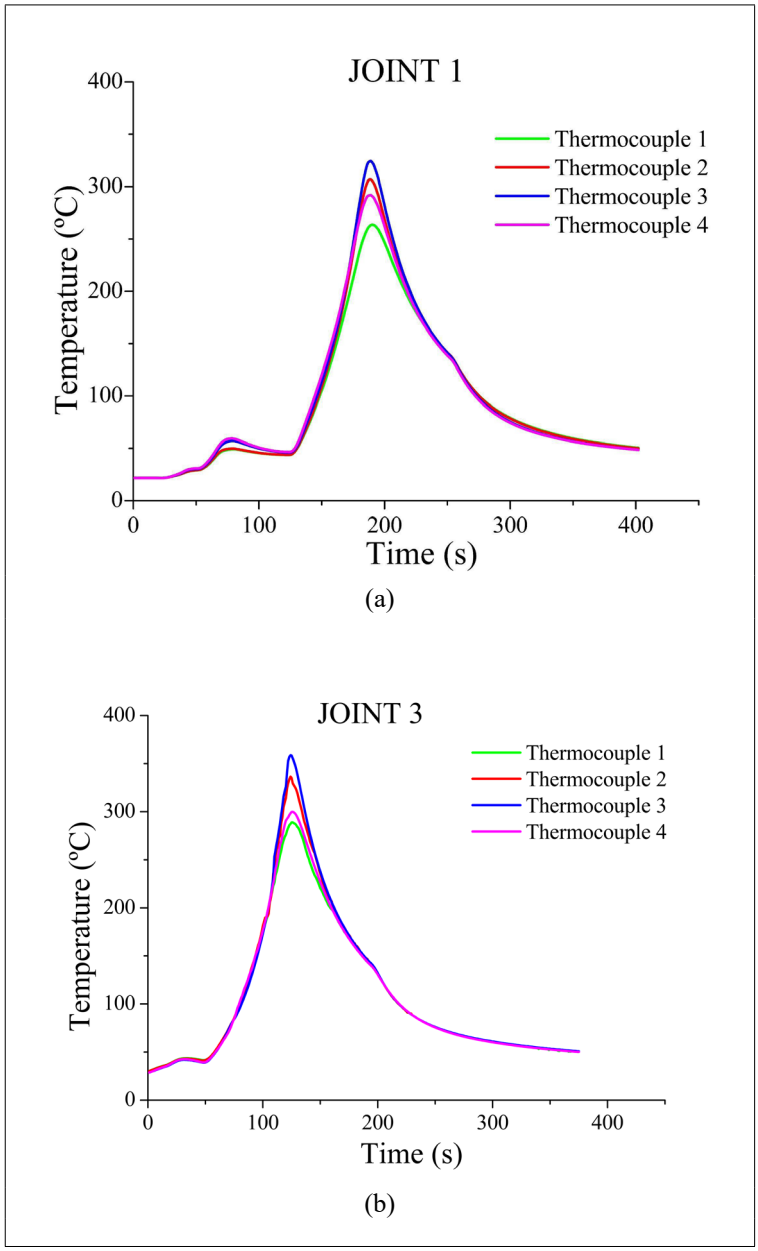

ISSN 2447-9187

Figure 5 ▶
Thermal cycles of joints 2 (a) and 4 (b).
Source: research data

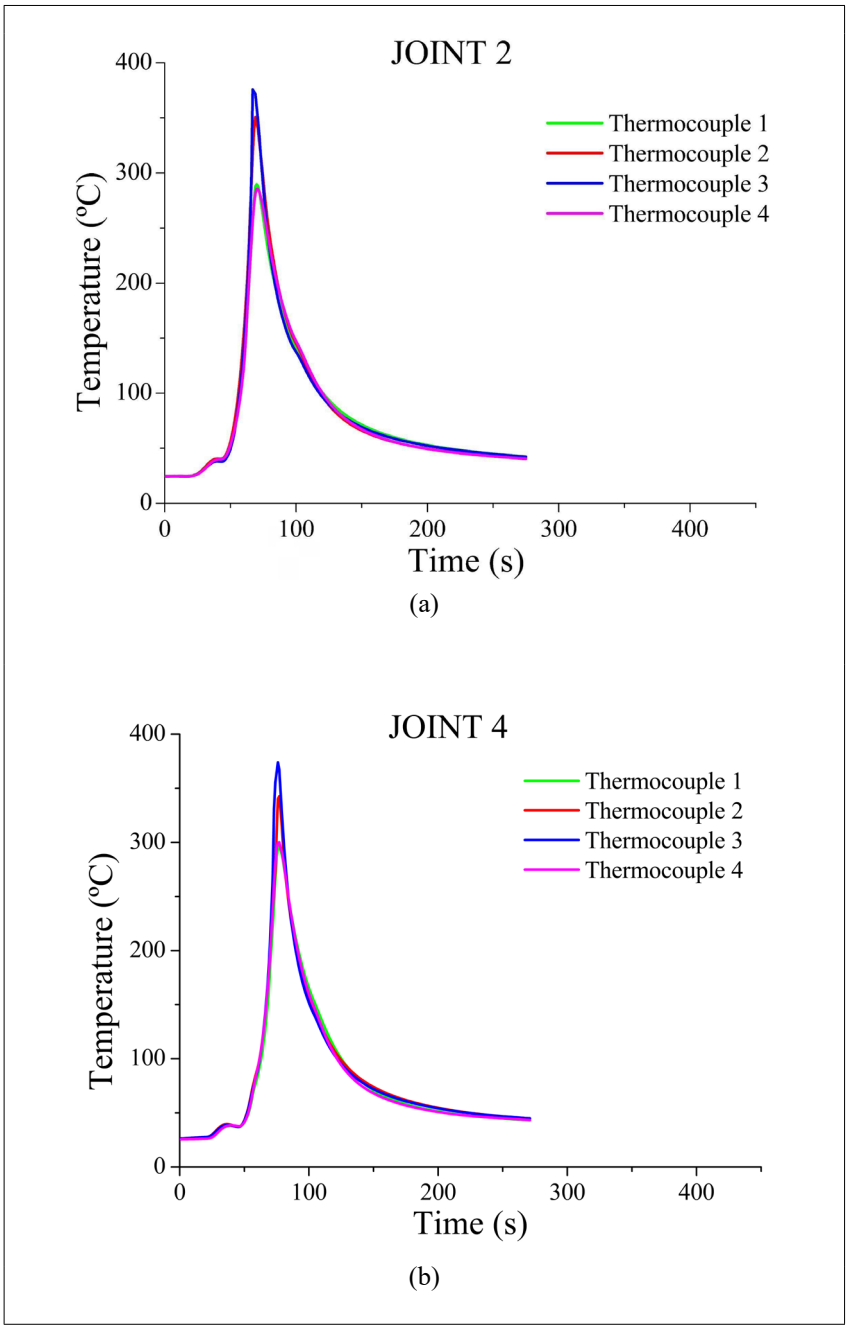

It was not feasible to determine the peak temperature at the weld center due to the mechanical nature of the FSW process, which involves a rotating tool stirring the material. Installing a thermocouple in this region would result in its destruction upon tool contact, interrupting temperature data acquisition. Therefore, the central temperature was estimated using Equation 1, proposed by Arbergast and Hartley (1998 *apud* Commin *et al*., 2009), for aluminum alloys, based on the welding parameters.

$$T = Tm\left[K\left(\frac{\omega^2}{\upsilon . 10^4}\right)^{\alpha}\right] \quad (1)$$

where: T: temperature in the stir zone (in °C); T_m: melting temperature; K: empirical constant (0.65-0.75); α: is an empirical constant (0.011); ω: is the tool rotation

speed (in rpm); υ: is the welding speed (in mm/min). The values of K and α were adopted as recommended by Commin *et al*. (2009) and Qian *et al*. (2017).

FSW joints are classified as "cold," "intermediate," or "hot," depending on the combination of tool rotation speed (ω) and welding speed (υ), which directly affect heat input (Q), as defined in Equation 2 (Wiedenhoft *et al*., 2018):

$$Q = \frac{\omega}{\upsilon} \quad (2)$$

The temperature reached during FSW is governed by the ω/υ ratio. Increasing the rotation speed while keeping the welding speed constant raises the generated heat. Conversely, reducing the welding speed while maintaining the rotation speed constant produces a similar effect (Bisadi *et al*., 2013).

Thermal data acquisition enabled the calculation of peak temperatures, cooling rates, and heat input, which are summarized in Table 4.

Table 4 ▼
Peak temperature, stir zone temperature, cooling rate, heat input, and classification.
Source: research data

		Joint 1	Joint 2	Joint 3	Joint 4
Welding parameter	ω (rpm)	470	1,585	470	1,585
	υ (mm/min)	47	117	47	117
	θ (º)	1	1	3	3
Peak temperature (ºC)	T1	263.634	289.577	288.804	297.533
	T2	306.882	350.767	336.470	342.581
	T3	324.596	375.700	358.735	373.925
	T4	291.849	285.434	299.894	300.009
Stir zone temperature (°C)	Eq.1	443.481	444.973	443.481	444.973
Cooling rate (ºC/s)	T1	2.144	5.368	2.275	5.269
	T2	2.905	6.923	2.914	8.024
	T3	3.174	8.061	3.261	9.330
	T4	2.676	4.670	2.498	5.770
Heat input: $\frac{\omega}{\upsilon}$	Eq.2	10	13.5	10.0	13.5
Classification of heat input		Cold	Cold	Cold	Cold

ω = tool rotation speed; υ = welding speed; θ = tool tilt; T1-T4 = Thermocouple 1 to 4

The highest peak temperatures were observed at thermocouple T3, located on the advancing side of the tool, as a result of increased mechanical action in this region. Similar findings were reported by Verma *et al*. (2025), where a thermocouple positioned

closest to the stir zone on the advancing side recorded the highest temperature. Therefore, higher tool rotation speeds correlate with elevated peak temperatures, as the vector of material engagement aligns with the tool speed vector, maximizing mechanical work and, consequently, heat generation and material flow. This behavior is contrary to the tangential velocity on the retreating side (Ni *et al*., 2019).

Temperature differences between the advancing and retreating sides ranged from 18 °C at lower welding and rotation speeds with a 1° tilt to 24 °C with a 3° tilt. For higher rotation and welding speeds, the temperature differences were 25 °C (1° tilt) and 31 °C (3° tilt). These findings suggest that greater tool tilt increases the pressure in the stir zone, thereby enhancing both temperature and mechanical work. According to Sinhmar and Dwivedi (2019), the tool shoulder is primarily responsible for heat generation in FSW, and an increased tilt angle amplifies this effect.

The pronounced thermal gradient between the advancing and retreating sides can result in uneven hardness profiles due to inconsistent thermal distribution across the weld width.

Joints 2 and 4 experienced more severe cooling rates, which suppressed phase transformations, as evidenced by secondary peaks in Figure 4 around 130 ºC to 140 ºC. Kalinenko *et al*. (2021) observed that higher cooling rates increase the likelihood of microstructural changes during the weld's cooling cycle.

All joints exhibited a slight change in curve concavity during cooling, manifested as a secondary peak, at temperatures detailed in Table 5.

Table 5 ▶
Temperature ranges at which phase transformations occurred during cooling.
Source: research data

	Temperature range
Joint 1	139.2 ºC to 135.1 ºC
Joint 2	143.4 ºC to 141.3 ºC
Joint 3	145.8 ºC to 143.7 ºC
Joint 4	152.8 ºC to 147.8 ºC

This inflection is attributed to the precipitation of a compact hexagonal Zn phase along the grain boundaries of face-centered cubic (FCC) aluminum. This phenomenon was identified by Jiang *et al*. (2018) in the AA7075 phase diagram for an 89% aluminum composition. Upon cooling, a phase transformation from Al-5 to Al-5 + 5 occurs.

In precipitation-hardened aluminum alloys, welding temperature significantly influences second-phase behavior, including dissolution, thickening, or precipitation. These phenomena can result in substantial degradation of the alloy's mechanical properties (Jiang *et al*., 2018).

3.3 Macro and microstructural analysis

Welds produced by the FSW process may exhibit defects resulting from the welding conditions and, consequently, from the thermal cycles experienced during processing. In this context, defects such as wormholes, kissing bonds, and lack of mixing were identified, as illustrated in Table 6.

ISSN 2447-9187

Table 6 ▼
Macrography of the cross-section of all joints.
Source: authors' archive

	Defects			
Joint	**Macrography**	**Wormhole**	**Kissing bond**	**Lack of mixing**
1	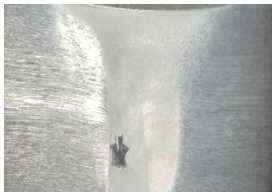	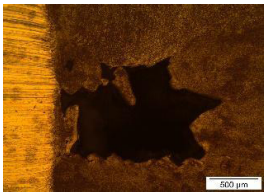	Not observed	Not observed
2	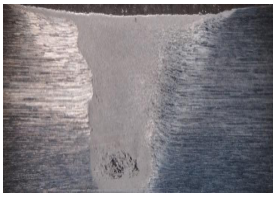	Not observed	Not observed	
3	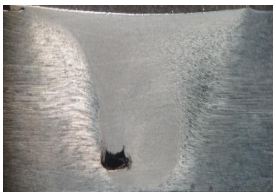		Not observed	Not observed
4		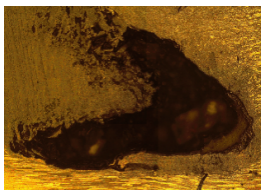	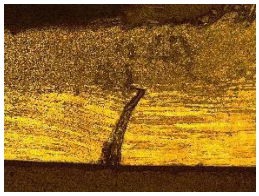	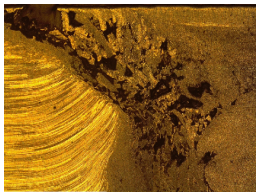

The macrographs of the four welded joints revealed defects that were not detected during the visual inspection. Wormhole defects were observed in three out of the four joints, with joint 2 being the only one without this defect. Joint 2 exhibited higher traverse and rotation speeds compared to joints 1 and 3, and a smaller tool tilt angle compared to joint 4.

A lack of mixing was identified in the stir zones of joints 2 and 4, resulting in defective joints with multiple cracks. According to Lima *et al*. (2022) such defects are attributed to abnormal material flow during welding, which may be caused by suboptimal combinations of process parameters, including tool rotation speed, welding speed, heat generation, and axial force applied by the tool shoulder. Notably, these joints also presented the highest recorded temperatures, which can be linked to their elevated traverse and rotation speeds.

In the case of joint 4, a microstructural defect known as a kissing bond was observed. At this location, proper metallurgical bonding between the plates was not achieved, resulting in a weak region susceptible to fracture. This imperfection typically occurs at the weld root and is characterized by a fragile interface adhesion that significantly reduces joint strength and may lead to premature failure (Taheri *et al*., 2019). In agreement

with this finding, joint 4 exhibited the lowest tensile strength, fracturing prematurely at 176.217 MPa.

The temperatures observed during the thermal welding cycles appear to be critical factors in defect formation. Joints 2 and 4, which exhibited the most significant defects, were also those that reached the highest peak temperatures and experienced the fastest cooling rates. It can thus be hypothesized that high peak temperatures combined with rapid cooling in solid-state welding processes may contribute to the formation of welding defects.

In friction stir welding (FSW), heat generation is directly proportional to parameters such as welding speed, tool rotation speed, shear stress, friction coefficient, and the contact force between the tool and the workpiece (Bhukya *et al*., 2023).

The temperature distribution across the plates is primarily governed by the amount of heat generated by the tool. Accordingly, a comprehensive understanding of the thermal history at the weld joint is essential, as it not only influences the formation of sound joints under solid-state conditions but also affects material flow, microstructure, precipitate morphology, and mechanical properties (Jeenjitkaew, 2011).

3.4 Vickers hardness

Figure 6 presents the Vickers hardness profiles measured along the cross-sections of the four welded joints. Notably, two of the hardness measurement points, specifically in joints 2 and 4, were situated near wormhole defects. These defects resulted in a significant drop in hardness at these locations, where the indentations were positioned very close to the defects, as indicated in the second and fourth conditions in Table 6.

Figure 6 ▼
Vickers hardness profile of the four welded joints.
Source: research data

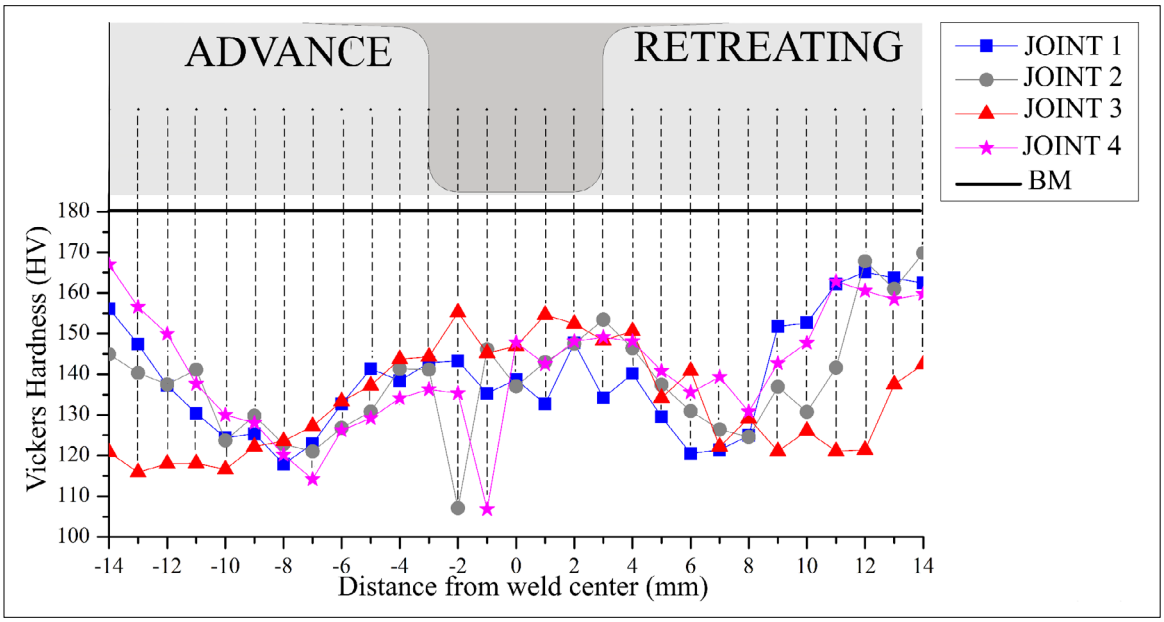

The results reveal considerable variation in the hardness profiles of the joints, displaying a characteristic "W" pattern. This pattern indicates a significant decrease in hardness levels in the regions adjacent to the SZ, which correspond to the TMAZ and the HAZ. A similar behavior was reported by Lima *et al*. (2022), who attributed the hardness reduction in these zones to localized heating and the mechanical deformation

imposed by the tool shoulder, which promoted grain growth and elongation. These microstructural changes lead to lower hardness values compared to the SZ (Ni *et al*., 2022).

In heat-treatable alloys, hardness typically diminishes as peak temperatures rise within the heat-affected regions (Lima *et al*., 2022). No significant hardness variation was observed among the different joints. The average Vickers hardness values for the SZ in each joint are listed in Table 7.

Table 7 ▶
Average Vickers hardness of the stir zone for the four welded joints.
Source: research data

Joint	Average hardness (HV)
1	138.7
2	143.0
3	148.3
4	142.5
Base metal	180.0

3.5 Uniaxial tensile strength

Figure 7 ▼
Tensile stress-strain curve of the four welded joints and the base metal.
Source: research data

Figure 7 presents the stress-strain curves for the base metal (BM) and the four welded joints. The variations observed in tensile strength values, as well as the significant reduction compared to the base metal, can be attributed to differences in heat input during each welding process, resulting from the specific combination of welding parameters, as previously shown in Table 6.

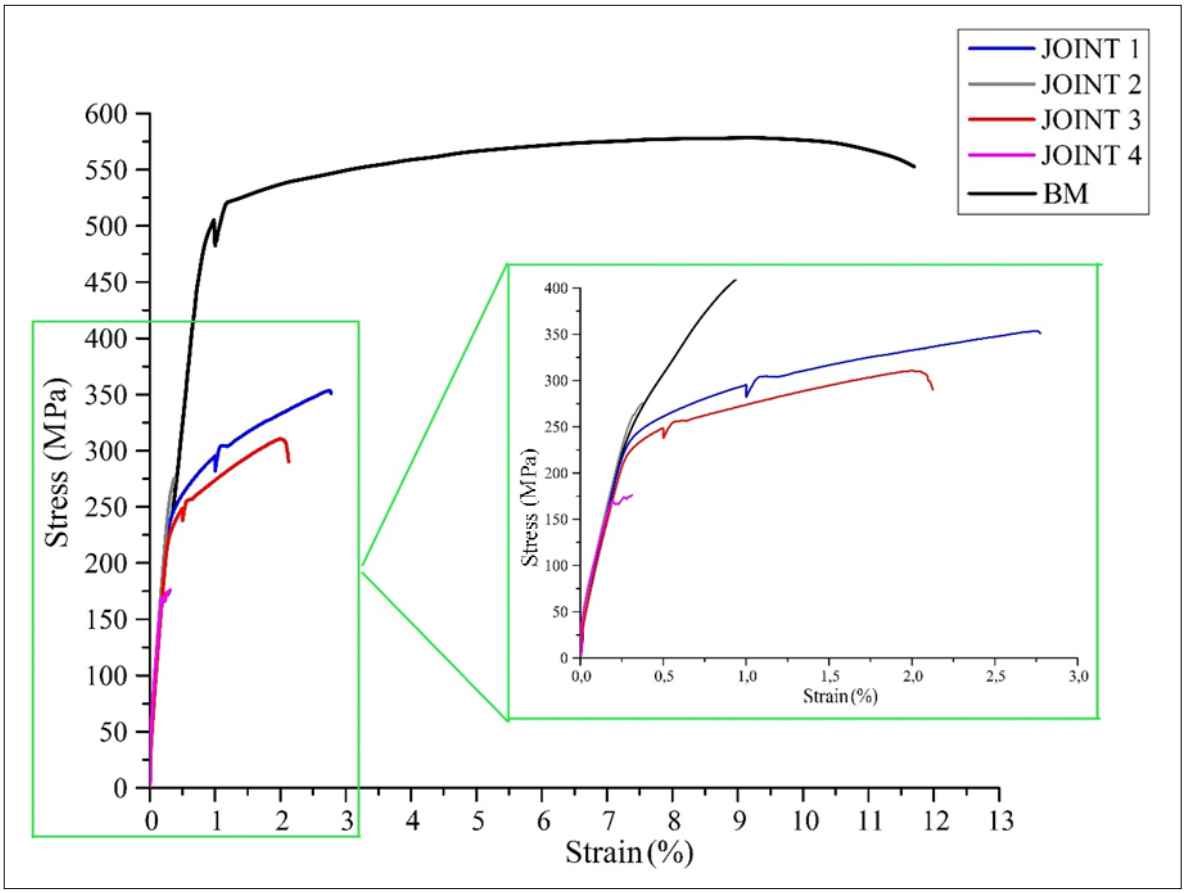

The measured values are summarized in Table 8, which presents the process temperatures, ultimate tensile strength (UTS), maximum deformation, and efficiency of each welded joint. The efficiency of each joint was calculated as the ratio between the UTS of the welded joint and that of the base metal, as shown in Equation 3.

$$\text{Efficiency } (\%) = \frac{UTS_{welded\ \ joint}}{UTS_{base\ \ metal}} \quad (3)$$

Table 8 ▼
Theoretical temperature, peak temperature, ultimate tensile strength, strain, and efficiency of each joint.
Source: research data

Joints 1 and 3 exhibited higher UTS values than joints 2 and 4. Analysis of the welding parameters indicates that joints 1 and 3 were produced using lower welding and rotation speeds, resulting in lower peak temperatures and slower cooling rates.

Joint	Theoretical temperature (ºC)	T3 – Peak temperature (ºC)	UTS (MPa)	Maximum deformation (%)	Efficiency (%)
1	394.469	324.596	353.602	2.77	60.0
2	428.712	375.700	275.510	0.37	47.8
3	394.469	358.735	310.742	2.13	53.9
4	428.712	373.925	176.217	0.31	29.5
BM	–	–	589.330	11.7	100

The joints that reached the highest peak temperatures also exhibited faster cooling rates, which correlated with lower tensile strength and a greater occurrence of surface defects and internal flaws. It was observed that increasing the tool's rotation speed led to a reduction in tensile strength due to the higher heat input.

3.6 Fractographic analysis

Detailed fractographic analyses were conducted on the fracture surfaces of the tensile-tested welded joints. The results are shown in Table 9 (next page), with images captured at magnifications of 100×, 500×, and 1000×.

ISSN 2447-9187

Table 9 ▼
Fractography of joints 1, 2, 3 and 4 at 100×, 500× and 1000× magnifications.
Source: authors' archive

	100×	500×	1000×
Joint 1	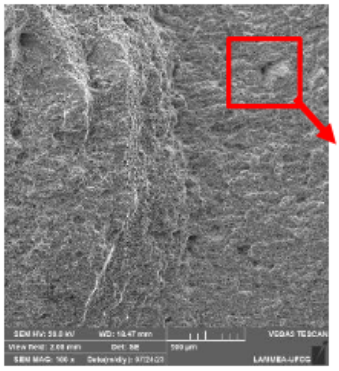	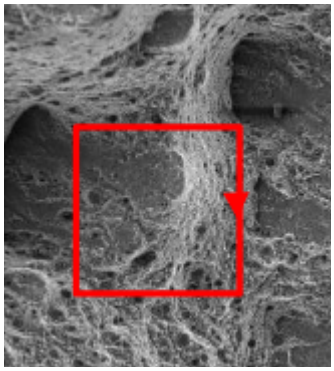	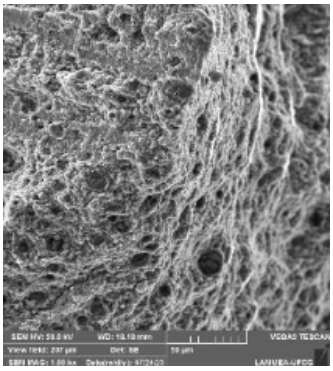
Joint 2	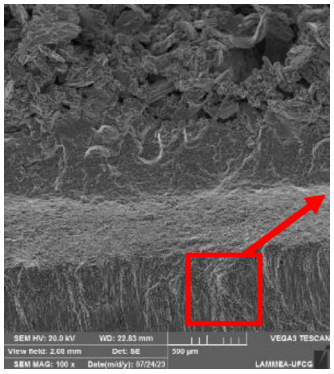	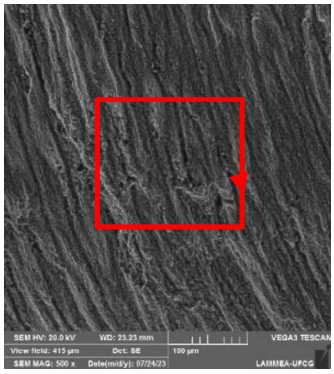	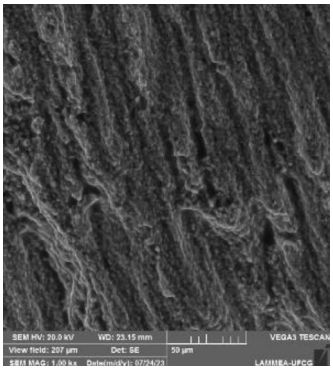
Joint 3	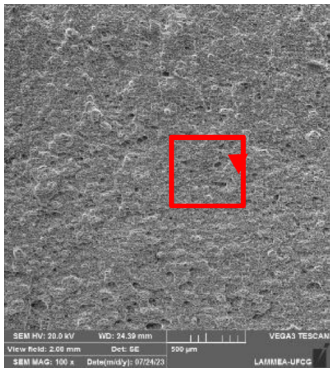	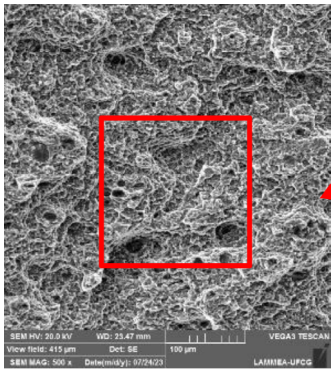	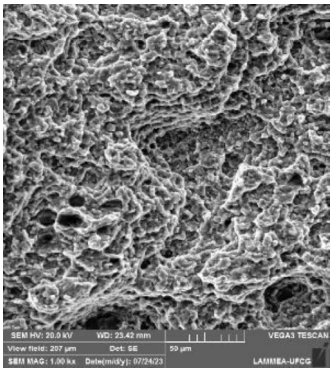
Joint 4	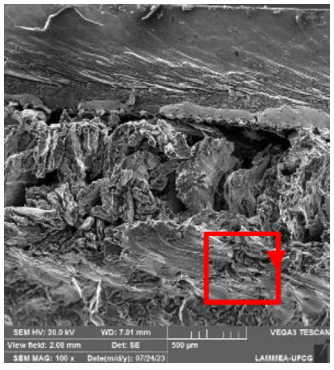	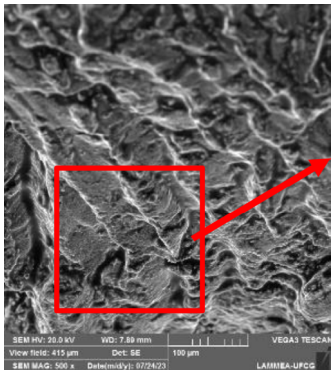	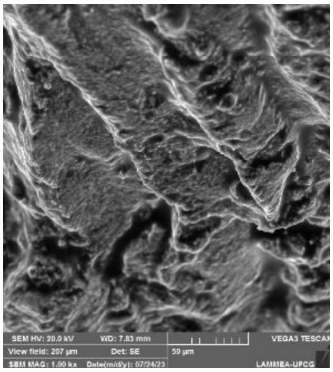

Joints 1 and 3 displayed features indicative of ductile fracture, characterized by substantial plastic deformation. In such fractures, the material resists rupture more effectively and undergoes significant plastic deformation before failure. Typically, ductile fractures result in localized necking in the stressed region (Ni *et al*., 2022).

In the same joints, numerous microvoids were observed, along with the absence of flat fracture surfaces. The presence of dimples and rough fracture features was also noted. These characteristics are typically associated with lower peak temperatures and slower heating and cooling rates than those observed in joints 2 and 4. Reduced cooling rates may have promoted phase precipitation, contributing to improved mechanical strength and favoring microductile fracture mechanisms. Conversely, joints 2 and 4 displayed features characteristic of brittle fracture, including a predominance of cracking with limited plastic deformation.

The differing fracture mechanisms can be attributed to the thermal inputs experienced during welding and the extent of phase transformation during cooling. In joints 1 and 3, the presence of such transformations, absent in joints 2 and 4 due to their higher cooling rates, appears to have contributed positively to joint ductility.

4 Conclusions

Regarding the visual appearance, welded joints produced at lower welding speeds (48 mm/min) and lower rotational speeds (470 rpm) exhibited superior surface quality. Additionally, larger tool tilt angles (1° and 3°) contributed to improved surface finish. Conversely, welds performed at higher welding speeds (117 mm/min) and higher rotational speeds (1,585 rpm) presented more pronounced burr formation.

In terms of the thermal cycle, higher peak temperatures and faster cooling rates were recorded for joints welded at higher speeds and rotations, whereas the lowest temperatures were observed in joints produced at lower welding speeds and tool rotations.

Macroscopic analysis revealed defects in all welded joints. The most common defect was the presence of wormholes, identified in three of the four joints (excluding joint 2), along with insufficient material mixing in some regions. Joints welded at lower travel and rotation speeds, combined with greater tool tilt angles, exhibited higher average hardness values in the stir zone (148.3 HV), which corresponds to approximately 82% of the base metal hardness.

The uniaxial tensile test results indicated that joints 1 and 3 exhibited the best mechanical performance. These joints were welded at lower speeds and rotations, which resulted in reduced peak temperatures and slower cooling rates. In contrast, joints welded at higher parameters showed limited plastic deformation before fracture. Fractographic analysis revealed ductile fracture characteristics in joints 1 and 3, while joints 2 and 4 displayed features associated with brittle fracture.

In summary, the investigation of welding thermal cycles demonstrated that high tool rotational speeds combined with high welding speeds negatively affected the joint quality produced by the FSW process for this alloy. The elevated temperatures associated with these parameters increased the cooling rate, which in turn altered the microstructure of the welded joint.

For future research, it is proposed to analyze welding thermal cycles across a broader range of parameters, as well as to investigate the influence of different tool

profiles. Furthermore, the development of a welding tool equipped with an embedded thermocouple is planned, enabling direct thermal cycle measurements within the stir zone, thus creating an intelligent tool.

Acknowledgments

This research was funded by the Fundação de Amparo à Pesquisa do Estado da Paraíba (FAPESQ/PB). The authors gratefully acknowledge the Instituto Federal da Paraíba (IFPB), Itabaiana campus, for providing the necessary infrastructure for fabricating the friction stir-welded joints. Appreciation is also extended to the Assert Laboratory for providing the equipment used to record the thermal cycles, and to the Federal University of Campina Grande (UFCG) for offering facilities for mechanical characterization and scanning electron microscopy (SEM) analysis.

Funding

One of the authors (R.H.F.M.) acknowledges financial support from the Fundação de Amparo à Pesquisa do Estado da Paraíba under the PPP Call No. 010/2021 FAPESQ/PB – MCTIC/CNPq (Grant Agreement No. 3200/2021).

Conflict of interest

The authors declare that there is no conflict of interest.

Note

This article is derived from a master's dissertation from the Graduate Program in Mechanical Engineering at the Federal University of Campina Grande (UFCG), available at: http://dspace.sti.ufcg.edu.br:8080/jspui/handle/riufcg/37586.

Author contributions

SANTOS, O. C.: responsible for performing the welding procedures and acquiring the thermal cycle data. **SOUZA, J. W. A.:** conducted the metallographic preparation and analysis. **MACIEL, T. M.; SANTOS, M. A.; MELO, J. B. C. A.:** contributed to the writing and discussion of the results related to metallurgy, fracture, and microstructure, respectively. **MELO, R. H. F.:** he was the master's advisor, secured funding for the project, structured the article, and supervised all revisions. All authors contributed to the writing, discussion, review, and approval of the final version of the manuscript.

References

AKBARI, M.; ASADI, P.; SADOWSKI, P. A review on friction stir welding/processing: numerical modeling. **Materials**, v. 16, n. 17, 5890, 2023. DOI: https://doi.org/10.3390/ma16175890.

ARDIKA, R. D.; TRIYONO, T.; MUHAYAT, N.; TRIYONO. A review porosity in aluminum welding. **Procedia Structural Integrity**, v. 33, p. 171-180, 2021. DOI: https://doi.org/10.1016/j.prostr.2021.10.021.

BHUKYA, S. N.; WU, Z.; ELMUSTAFA, A.; AL-ALLAQ, A.; OJHA, M.; MOHAMMED, Y. Cu donor material assisted friction stir welding of AA2024 and AA6061 dissimilar alloys: effect on downward force, temperature profile, and mechanical properties. **The International Journal of Advanced Manufacturing Technology**, v. 127, p. 3839-3851, 2023. DOI: https://doi.org/10.1007/s00170-023-11778-3.

BISADI, H.; TAVAKOLI, A.; SANGSARAKI, M. T.; SANGSARAKI, K. T. The influences of rotational and welding speed on microstructures and mechanical properties of friction stir welded Al5083 and commercially pure copper sheets lap joints. **Materials & Design**, v. 43, p. 80-88, 2013. DOI: https://doi.org/10.1016/j.matdes.2012.06.029.

BUGLIONI, L.; TUFARO, L. N.; SVOBODA, H. G. Thermal cycles and residual stresses in FSW of aluminum alloys: experimental measurements and numerical models. **Procedia Materials Science**, v. 9, p. 87-96, 2015. DOI: https://doi.org/10.1016/j.mspro.2015.04.011.

CINTRA FILHO, J. P.; ARAUJO FILHO, L.; ITIKAVA, R. K.; SILVA, M. M.; PEREZ, R. A. Thermomechanical modelling of FSW process using a cylindrical tool in an aluminum alloy alclad AA 2024-T3. **Materials Research**, v. 21, n. 4, e20170773, 2018. DOI: https://doi.org/10.1590/1980-5373-MR-2017-0773.

COLAÇO, D. B.; RIBEIRO, M. A.; MACIEL, T. M.; MELO, R. H. F. Characterization and evaluation of mechanical properties and residual stress in aluminum-magnesium alloys welded by the FSW process. **Materials Science Forum (MSF)**, v. 1012, p. 349-353, 2020. DOI: https://doi.org/10.4028/www.scientific.net/msf.1012.349.

COMMIN, L.; DUMONT, M.; MASSE, J.-E.; BARRALLIER, L. Friction stir welding of AZ31 magnesium alloy rolled sheets: Influence of processing parameters. **Acta Materialia**, v. 57, n. 2, p. 326-334, 2009. DOI: https://doi.org/10.1016/j.actamat.2008.09.011.

GAO, T.; YING, L.; HU, P.; HAN, X.; RONG, H.; WU, Y.; SUN, J. Investigation on mechanical behavior and plastic damage of AA7075 aluminum alloy by thermal small punch test: experimental trials, numerical analysis. **Journal of Manufacturing Processes**, v. 50, p. 1-16, 2020. DOI: https://doi.org/10.1016/j.jmapro.2019.12.012.

GULER, K. A.; KISASOZ, A.; OZER, G.; KARAASLAN, A. Cooling slope casting of AA7075 alloy combined with reheating and thixoforging. **Transactions of Nonferrous Metals Society of China**, v. 29, n. 11, p. 2237-2244, 2019. DOI: https://doi.org/10.1016/S1003-6326(19)65129-0.

JEENJITKAEW, C. **Kissing bonds in adhesive joints**: a holistic approach for surface chemistry and joint mechanics. 2011. Doctoral Thesis (Doctorate of Philosophy) – School of Engineering and Materials Science Queen Mary, University of London, London, 2011. Available at: https://core.ac.uk/works/8850473/. Accessed on: 25 May 2025.

JIANG, W.; JIANG, Z.; LI, G.; WU, Y.; FAN. Z. Microstructure of Al/Al bimetallic composites by lost foam casting with Zn interlayer. **Materials Science and Technology**, v. 34, n. 4, p. 487-492, 2018. DOI: https://doi.org/10.1080/02670836.2017.1407559.

KALINENKO, A.; VYSOTSKIY, I.; MALOPHEYEV, S.; MIRONOV, S.; KAIBYSHEV, R. Influence of the weld thermal cycle on the grain structure of friction-stir joined 6061 aluminum alloy. **Materials Characterization**, v. 178, 111202, 2021. DOI: https://doi.org/10.1016/j.matchar.2021.111202.

KIM, H.; LEE, K.; KIM, J.; LEE, C.; JUNG, Y.; KANG, S. A study on the friction stir welding experiment and simulation of the fillet joint of extruded aluminum material of electric vehicle frame. **Applied Sciences**, v. 10, n. 24, 9103, 2020. DOI: https://doi.org/10.3390/app10249103.

LI, Y.; ZHOU, Z.; YIN, L.; FU, D.; JIANG, H.; YANG, Y.; LU, J.; JIN, F. Thermal cycling, microstructure, and mechanical properties of Al-Mg-Si-Cu alloy bobbin tool friction stir welded joints based on thermal index. **Coatings**, v. 13, n. 9, 1607, 2023. DOI: https://doi.org/10.3390/coatings13091607.

LIMA, J. S.; SANTOS, O. C.; SILVA, A. A.; MELO, R. H. F.; MACIEL, T. M. Influence of welding parameters on the mechanical properties and microstructure of 7075-T651 aluminum alloys welded joint performed by FSW process. **Materials Research**, v. 25, e20210629, 2022. DOI: https://doi.org/10.1590/1980-5373-MR-2021-0629.

NI, Y.; LIU, Y.; ZHANG, P.; HUANG, J.; YU, X. Thermal cycles, microstructures and mechanical properties of AA7075-T6 ultrathin sheet joints produced by high speed friction stir welding. **Materials Characterization**, v. 187, 111873, 2022. DOI: https://doi.org/10.1016/j.matchar.2022.111873.

NI, Y.; MAO, Y.; QIN, D.; XIAO, X.; FU, L. Thermal cycles and deformation characters during high-speed micro friction stir welding process of AA7075-T6 sheets. **Metals**, v. 9, n. 11, 1236, 2019. DOI: https://doi.org/10.3390/met9111236.

QIAN, J.; OU, Y.; LI, J.; XIAO, Y.; WU, L.; XU, Y. An analytical model to calculate the peak temperature for friction stir welding. **Science and Technology of Welding and Joining**, v. 22, n. 6, p. 520-525, 2017. DOI: http://dx.doi.org/10.1080/13621718.2016.1268367.

SILVESTRI, A. T.; COZZOLINO, E.; ALTERIIS, G.; ASTARITA, A.; SCHIANO LO MORIELLO, R.; SQUILLACE, A. Monitoring of the friction stir welding process: A preliminary study. **Materials Research Proceedings**, v. 41, p. 2891-2900. 2024. DOI: https://doi.org/10.21741/9781644903131-316.

SINHMAR, S.; DWIVEDI, D. K. Effect of weld thermal cycle on metallurgical and corrosion behavior of friction stir weld joint of AA2014 aluminium alloy. **Journal of Manufacturing Processes**, v. 37, p. 305-320, 2019. DOI: https://doi.org/10.1016/j.jmapro.2018.12.001.

TAHERI, H.; KILPATRICK, M.; NORVALLS, M.; HARPER, W. J.; KOESTER, L. W.; BIGELOW, T.; BOND, L. J. Investigation of nondestructive testing methods for friction stir welding. **Metals**, v. 9, n. 6, 624, 2019. DOI: https://doi.org/10.3390/met9060624.

THREADGILL, P. L.; LEONARD, A. J.; SHERCLIFF, H. R.; WITHERS, P. J. Friction stir welding of aluminium alloys. **International Materials Reviews**, v. 54, n. 2, p. 49-93, 2009. Available at: https://www.twi-global.com/technical-knowledge/published-papers/friction-stir-welding-of-aluminium-alloys. Accessed on: 20 May 2025.

VERMA, S.; WU, C. S.; THAKUR, L.; MUHAMMAD, N. A.; LI, S. Material flow behavior and thermal cycle during friction stir welding of AA5083/AZ91 dissimilar metals. **Journal of Materials Engineering and Performance**, v. 34, p. 8707-8724, 2025. DOI: https://doi.org/10.1007/s11665-024-10374-0.

WIEDENHOFT, A. G.; AMORIM, H. J.; ROSENDO, T. S.; TIER, M. A. D.; REGULY, A. Effect of heat input on the mechanical behaviour of Al-Cu FSW lap joints. **Materials Research**, v. 21, n. 4, e20170983, 2018. DOI: https://doi.org/10.1590/1980-5373-MR-2017-0983.

WU, T.; ZHAO, F.; LUO, H.; WANG, H.; LI, Y. Temperature monitoring and material flow characteristics of friction stir welded 2A14-T6 aerospace aluminum alloy. **Materials**, v. 12, n. 20, 3387, 2019. DOI: https://doi.org/10.3390/ma12203387.

YANG, C.; NI, D. R.; XUE, P.; XIAO, B. L.; WANG, W.; WANG, K. S.; MA, Z. Y. A comparative research on bobbin tool and conventional friction stir welding of Al-Mg-Si alloy plates. **Materials Characterization**, v. 145, p. 20-28, 2018. DOI: https://doi.org/10.1016/j.matchar.2018.08.027.